Electronic Supplementary Information

Chemicals and materials

Iridium chloride hydrate ($IrCl_3 \cdot xH_2O$), cobalt (II) nitrate hexahydrate ($Co(NO_3)_2 \cdot 6H_2O$), *N*, *N*-dimethylformamide (DMF/$HCON(CH_3)_2$) were supplied by Alfa Aesar. 1,4-Benzenedicarboxylic acid (BDC/$C_8H_6O_4$), triethylenediamine (TED/$C_6H_{12}N_2$), ruthenium oxide (RuO_2), and commercial Pt/C (20 wt%) were provided from Sinopharm Chemical Reagent Co. Ltd. (Shanghai, China). Potassium hydroxide (KOH, ACS), D-(+)-glucose ($C_6H_{12}O_6$), deuterium oxide (D_2O), and maleic acid ($C_4H_4O_4$) were purchased from Aladdin Industrial Corporation (Shanghai, China). All chemicals were used as received without any further purification. Deionized water from a Smart -S15 water purification system was used in all experiments (Shanghai, China).

Synthesis of the CoIr-MOF/NF

Pretreatment of commercial Ni foam was carried out by soaking it in HCl (3 M) to remove the surface oxide layer (15 min), and then, washed with ethanol and water alternately. For synthesis of typical CoIr-MOF/NF, 0.105 g of BDC, 0.033 g of TED, and 0.3 g of Co $(NO_3)_2 \cdot 6H_2O$ were dissolved in N, N-dimethylformamide (DMF, 30 mL) with ultrasonication to form a homogeneous and transparent pink solution. Subsequently, a $IrCl_3$ aqueous solution (2 mL, 20 mM) was added dropwise into the above homogeneous solution under vigorous stirring and continued to stir for 15 minutes. Finally, the reaction solution and the pretreated Ni foam (1 x 2 cm^2) were transferred to a 50 ml Teflon-lined autoclave, which was heated for 24 h at 130 °C. Ultimately, the as-synthesized CoIr-MOF/NF washed with ethanol and dried at 50 °C. The Co-MOF/NF counterpart was synthesized by similar procedure except that the $IrCl_3$ aqueous solution was replaced with an equal amount of deionized water.

General characterization

The morphology features of catalysts can be identified in the scanning electron microscopy (SEM: Gemini SEM 500) images and the transmission electron microscopy (TEM: FEI Tecnai F20) images. The phase of electrocatalysts was performed by X-ray diffraction (XRD: Ultima IV) spectra. The compositions and surface chemistry valence state of catalysts were analyzed by energy dispersive x-ray spectroscopy (EDX) and X-ray photoelectron spectroscopy (XPS: Thermo Kalpha) analysis. Product identification and quantification were detected by a nuclear magnetic resonance (NMR: Bruker Avance IIIHD500) spectrometer.

Electrochemical measurements

The electrocatalytic performance for HER, GOR, and OER of the CoIr-MOF/NF were investigated on a 660E workstation (CH Instruments). The self-supporting CoIr-MOF/NF (1 cm×1 cm), graphite rod, and Ag/AgCl electrode were respectively used as working, counter and reference electrodes to construct a typically three-electrode system. In electrochemical studies, bare NF, Co-MOF/NF, Pt/C/NF (commercial 20 wt% Pt/C loaded on NF: 1.5 mg cm^{-2}), RuO_2/NF (commercial RuO_2 loaded on NF: 1.5 mg cm^{-2}) were employed as contrastive catalysts. The voltages during the tests were all converted to the reversible hydrogen electrode (RHE: $E_{vs.\ RHE} = E^0_{Ag/AgCl} + E_{vs.\ Ag/AgCl} + 0.059\times pH$). Linear sweep voltammetry (LSV) curves were measured at a sweep speed of 5 mV s^{-1}. All of the polarization curves were iR corrected. Electrochemical impedance spectroscopy (EIS) was performed in a frequency range from 10^5 Hz to 10^{-1} Hz with an amplitude of 5 mV. The electrochemical active surface area (ECSA) of the catalyst was calculated by double layer capacitance (C_{dl}) and working electrode's geometric surface area according to the following equation:

$$\text{ECSA} = (\text{geometric surface} \times C_{dl}) / \text{specific}\, C_{dl}$$

Where the specific C_{dl} value is 0.040 mF cm^{-2} based on the literature.[1, 2]

The amount of H_2 produced was evaluated by using the drainage method, and the amount of formate produced was measured by using ^1H NMR spectroscopy. As a supplement, the H-type electrolytic cell is used for the H_2 production test and the others are all electrolytic cells without diaphragms. The FE (%) is calculated by the charge passed through the electrode (Q), the moles of the product (N), and the moles of electrons transferred required to produce per mole of H_2 ($Z = 2$) or formate ($Z = 2$), as the following equation:

$$FE = \frac{N \times Z \times F}{Q} \times 100\%$$

where F is the Faraday constant (96485 C mol^{-1}).[3]

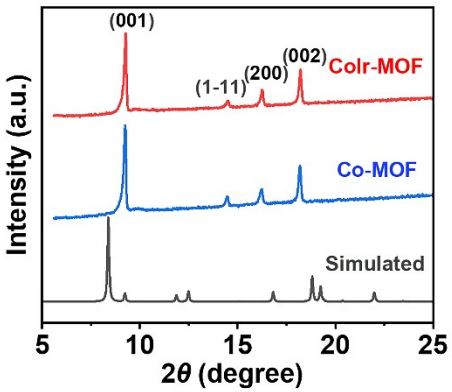

Fig. S1 XRD patterns of the Co-MOF and CoIr-MOF nanosheets.

The four diffraction peaks at about 9.3°, 14.5°,16.3 ° and 18.2° could be indexed to the (001), (1-11), (200) and (002) peaks of simulated XRD of the previously reported $M_2(BDC)_2TED$ MOF structure,[4] indicating the formation of highly oriented $M_2(BDC)_2TED$ MOF structure with preferential [001]-orientation.

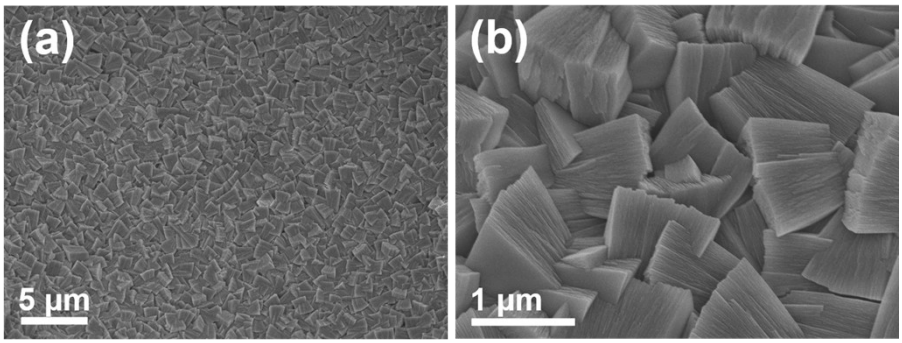

Fig. S2 SEM images of the Co-MOF/NF.

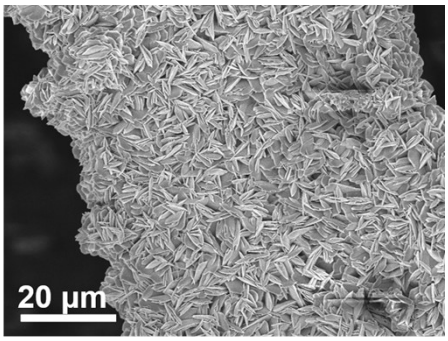

Fig. S3 SEM image of the CoIr-MOF/NF.

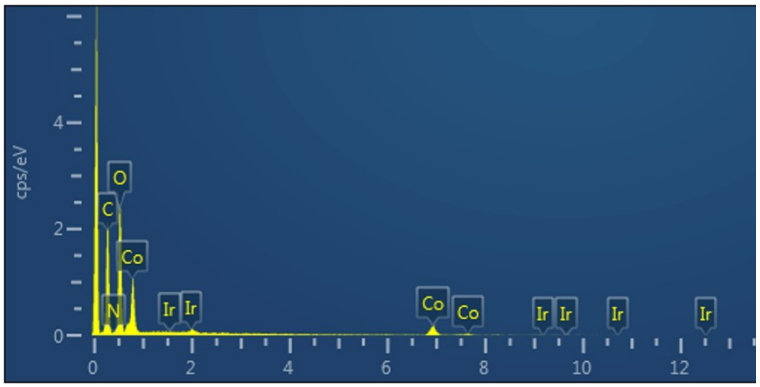

Fig. S4 EDS result of CoIr-MOF nanosheets.

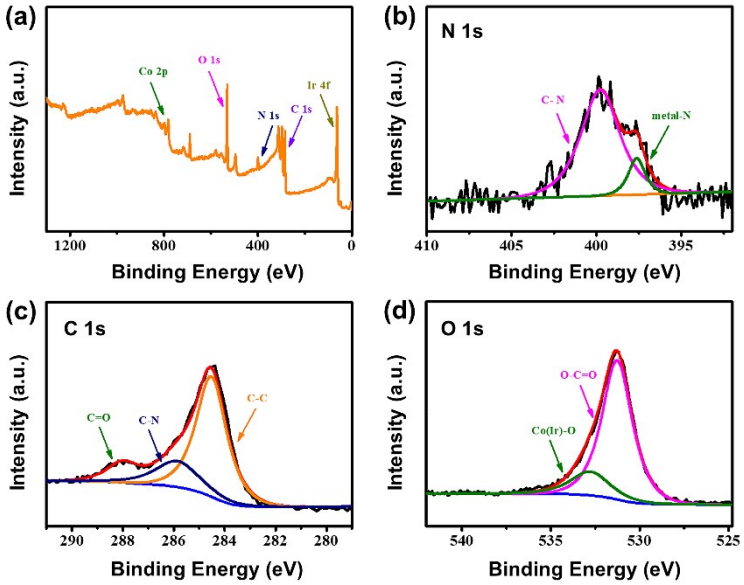

Fig. S5 (a) The XPS survey spectrum of the CoIr-MOF nanosheets. XPS profiles of (b) N 1s (c) C 1s, (d) O 1s in CoIr-MOF nanosheets.

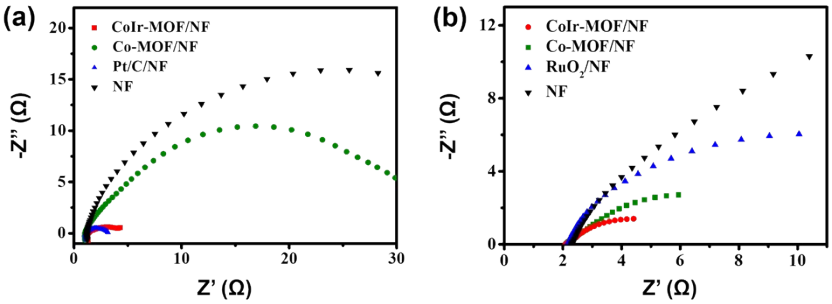

Fig. S6 Electrochemical impedance spectra of various catalysts in 1.0 M KOH with and without 0.1 M glucose under different applied potentials: (a) -0.05 V (vs. RHE), (b) 1.4 V (vs. RHE).

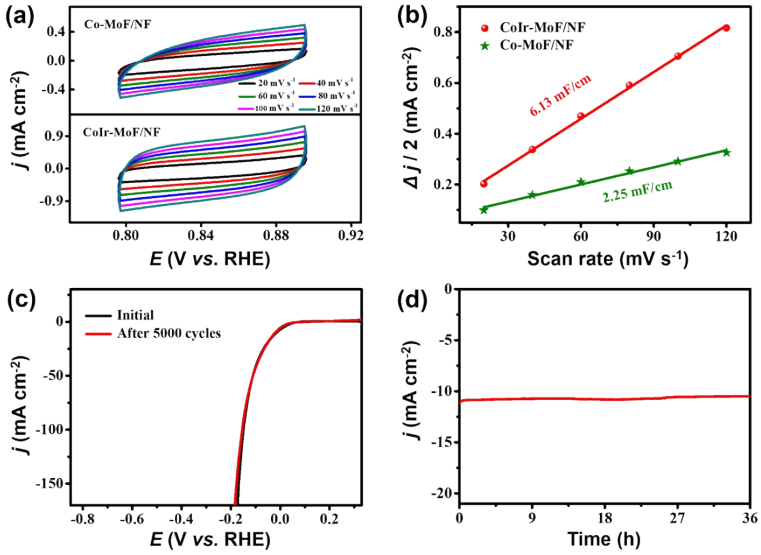

Fig. S7 (a) Electrochemical double-layer capacitance measurements of (a) CoIr-MOF/NF and Co-MOF/NF at scan rates of 20, 40, 60, 80, 100, and 120 mV s^{-1}. (b) Capacitive current densities as a function of scan rate for CoIr-MOF/NF and Co-MOF/NF at 0.845 V (vs. RHE). (c) Comparison of HER LSV curves of CoIr-MOF/NF catalyst before and after 5000 cycles CV test. (d) The i-t tests of CoIr-MOF/NF catalyst for 36 h at an overpotential of 50 mV.

As shown in Fig. S7a-b, the Cdl values for CoIr-MOF/NF and Co-MOF/NF were measured to be 6.13 mF cm^{-2} and 2.25 mF cm^{-2}, respectively. Accordingly, the ECSAs of CoIr-MOF/NF and Co-MOF/NF were calculated to be 153.3, and 56.2 cm^2, respectively,

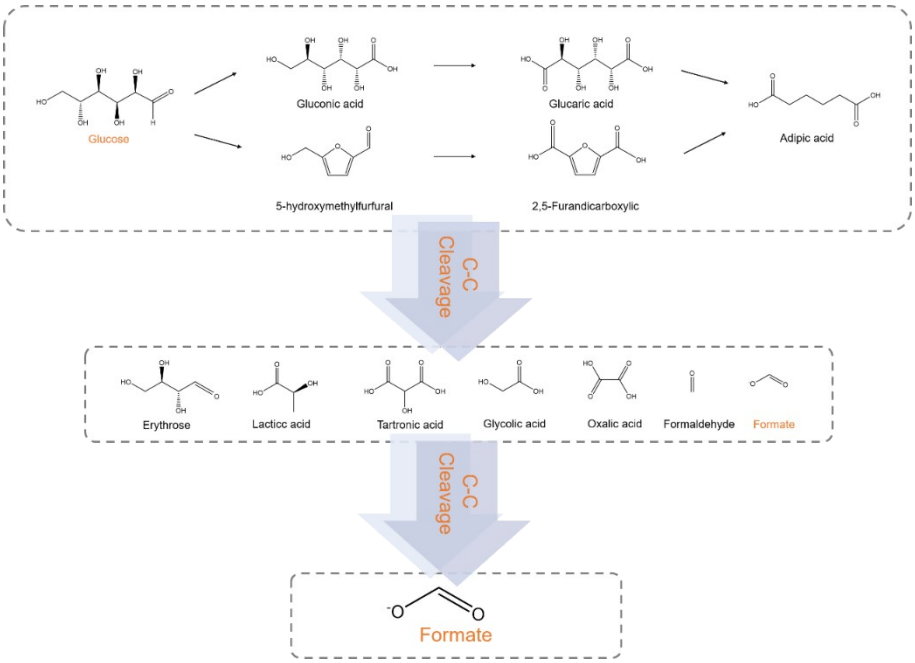

Fig. S8 Mechanistic scheme of glucose electro-oxidation to formate on CoIr-MOF/NF in alkaline medium.

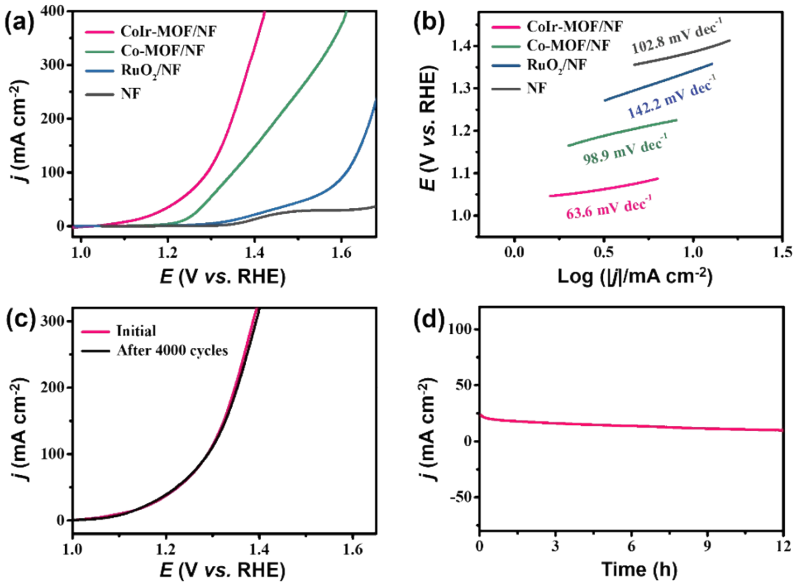

Fig. S9 (a) LSV curves of different electrodes for glucose oxidation in 1 M KOH with 0.1 M glucose. (b) Corresponding Tafel plots on various electrodes. (c) Comparison of LSV curves of CoIr-MOF/NF catalyst before and after 4000 cycles CV test. (d) The i-t tests of CoIr-MOF/NF catalyst at 1.30 V curve for 12 h.

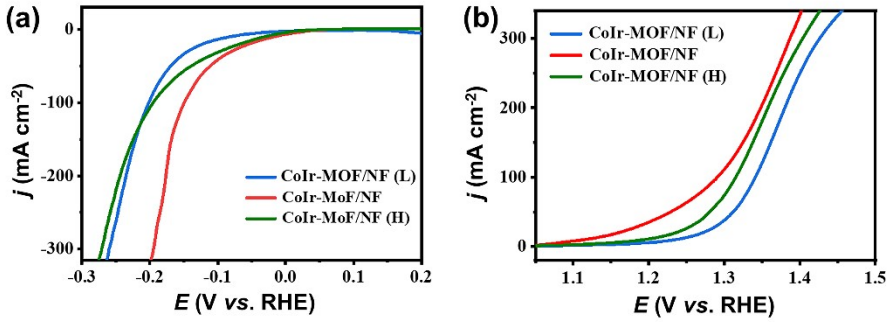

Fig. S10 (a) HER polarization curves and (b) GOR polarization curves for various CoIr-MOF catalysts with different Ir contents.

It can be observed from Fig. S10 that, increasing the adding amount of $IrCl_3$ precursor in the synthesis of MOF precursor from 0.02 mmol (denoted as CoIr-MOF/NF(L)) to 0.04 mmol (our typical CoIr-MOF/NF), both the HER and GOR performance of the resultant CoIr-MOF/NF catalyst could be enhanced. However, both the HER and GOR performance decreased with further increasing adding amount of $IrCl_3$ precursor to 0.06 mmol (denoted as CoIr-MOF/NF(H)).

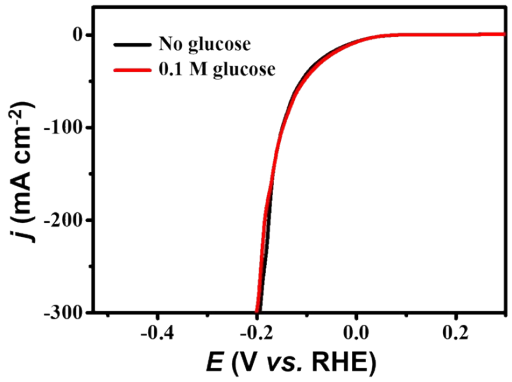

Fig. S11 HER polarization curves for CoIr-MOF/NF in 1 M KOH solution with and without 0.1 M glucose addition.

Fig. S12 The photograph of an electrochemical cell for the water-glucose co-electrolysis system.

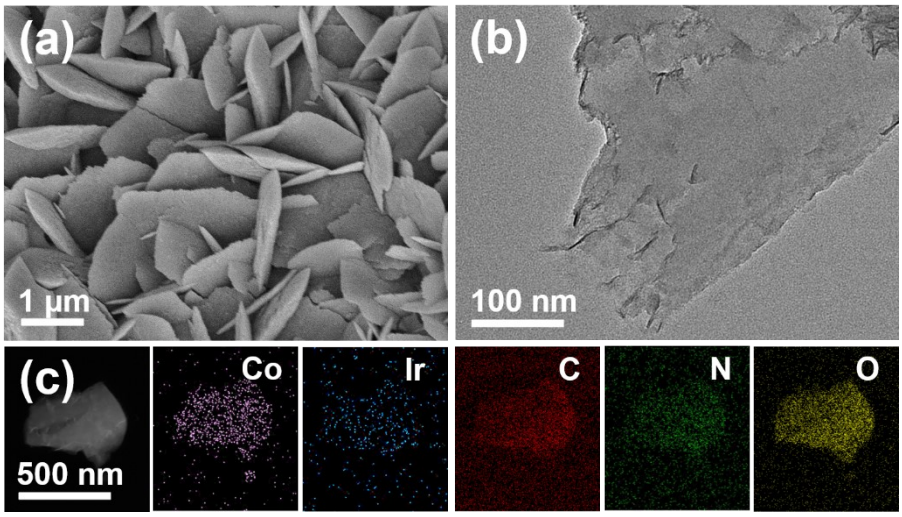

Fig. S13 (a) SEM image of the post-HER CoIr-MOF/NF. (b) TEM image, (c) HAADF-STEM and elemental mapping images of the post-HER CoIr-MOF nanosheets.

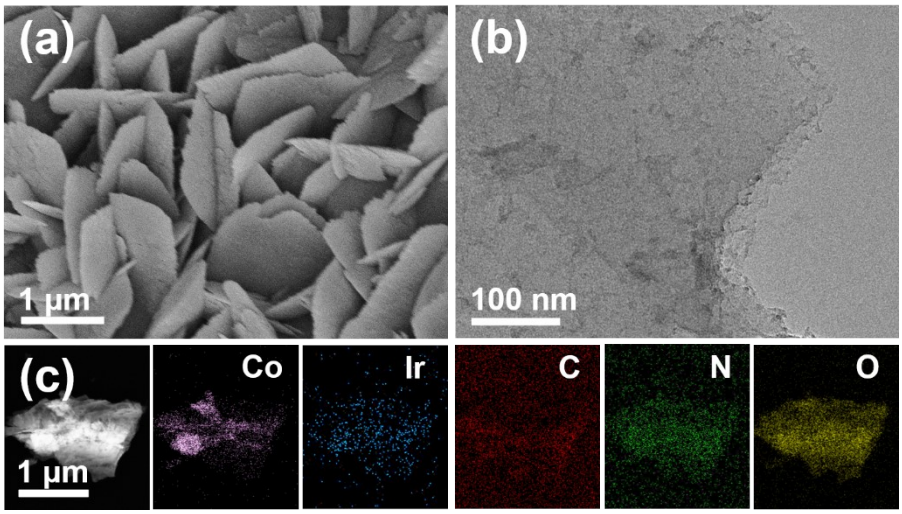

Fig. S14 (a) SEM image of the post-GOR CoIr-MOF/NF. (b) TEM image, (c) HAADF-STEM and elemental mapping images of the post-GOR CoIr-MOF nanosheets.

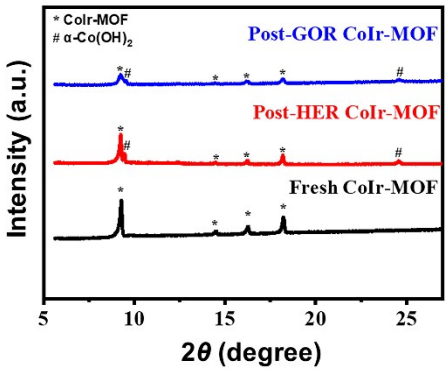

Fig. S15 XRD patterns of fresh, post-HER and GOR CoIr-MOF nanosheets.

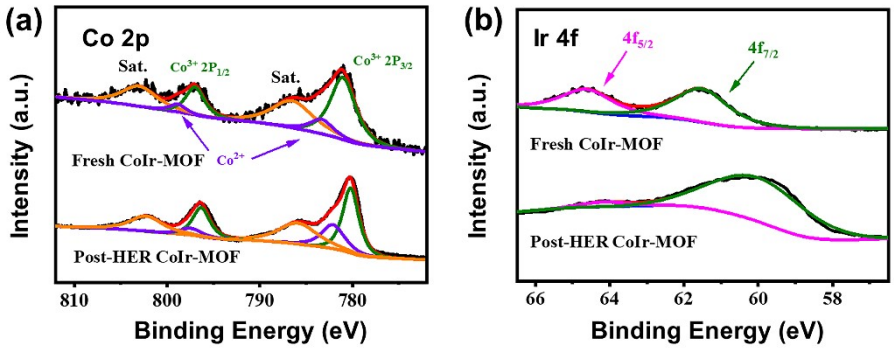

Fig. S16 High-resolution Co 2p (a) and Ir 4f (b) XPS spectra for fresh and post-HER CoIr-MOF nanosheets.

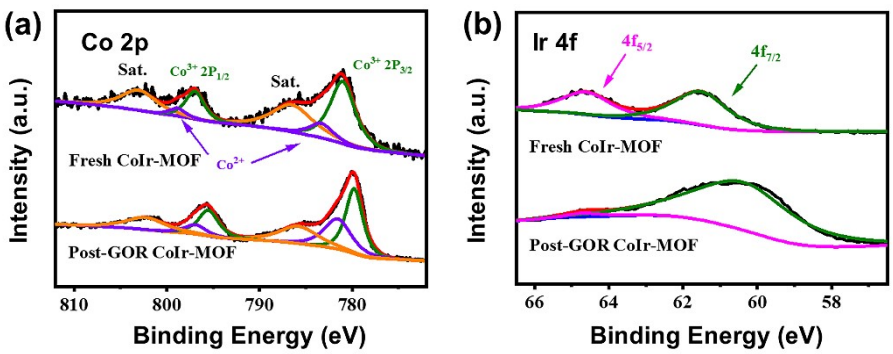

Fig. S17 High-resolution Co 2p (a) and Ir 4f (b) XPS spectra for fresh and post-GOR CoIr-MOF nanosheets.

Table S1. Comparison of cell voltages of Co-based electrocatalysts for selective oxidation-assisted hydrogen production.

Bifunctional catalysts	**Electrolyte**	**Main anode product**	**Cell voltage (V) 10 mA cm^{-2}**	**Ref.**
CoIr-MOF/NF	**1.0 M KOH+ 0.1 M glucose**	**formate**	**1.29**	**this work**
NC@$CuCo_2Nx$/CF	1 M KOH + 0.015 M benzyl alcohol	benzalzehyde	1.55	[5]
Co $(OH)_2$@HOS/CP	1 M KOH + 3 M methanol	formate	1.50	[6]
CoNi alloy	1 M KOH + 0.1 M glucose	gluconic acid	1.39	[7]
NiCoP/CC	1.0 M KOH + 0.5 M urea	N_2, CO_2	1.42	[8]
Co_3S_4-NSs/Ni-F	1 M KOH + 0.5 M ethanol	potassium acetate	1.48	[9]
Co-S-P/CC	1 M KOH + 1.0 M ethanol	acetic acid	1.63	[10]
Co−P/CF	1.0 M KOH + 50 mM 5-hydroxymethylfurfural	2,5-furandica-rboxylic acid	1.39	[11]
$CoMn/CoMn_2O_4$	1.0 M KOH + 0.5 m urea	N_2, CO_2	1.51	[12]
$Ni_{0.33}Co_{0.67}(OH)_2$/NF	1.0 M KOH + 0.5 M methanol	formate	1.50	[13]
CoxP@NiCo-LDH/NF	1 M KOH + 0.5 M methanol	formate	1.43	[14]
Ru-Co_2P/N-C	1.0 M KOH + 0.5 m urea	N_2, CO_2	1.34	[15]
$CoNi_{0.25}P$	1 M KOH + 0.3 M ethylene glycol	formate	1.32	[16]
$Co_{0.83}Ni_{0.17}$/AC	1.0 M KOH +10 mM benzyl alcohol	benzoic acid	1.43	[17]

References

1. H. Liu, J. Cheng, W. He, Y. Li, J. Mao, X. Zheng, C. Chen, C. Cui and Q. Hao, *Appl. Catal. B: Environ.*, 2022, **304**, 120935.
2. T. Ren, K. Ren, M. Wang, M. Liu, Z. Wang, H. Wang, X. Li, L. Wang and Y. Xu, *Chem. Eng. J.*, 2021, **426**, 130759.
3. Y. Xu, M. Liu, S. Wang, K. Ren, M. Wang, Z. Wang, X. Li, L. Wang and H. Wang, *Appl. Catal. B: Environ.*, 2021, **298**, 120493.
4. D.-J. Li, Q.-H. Li, Z.-G. Gu and J. Zhang, *J. Mater. Chem. A*, 2019, **7**, 18519-18528.
5. J. Zheng, X. Chen, X. Zhong, S. Li, T. Liu, G. Zhuang, X. Li, S. Deng, D. Mei and J.-G. Wang, *Adv. Funct. Mater.*, 2017, **27**, 1704169.
6. K. Xiang, D. Wu, X. Deng, M. Li, S. Chen, P. Hao, X. Guo, J. L. Luo and X. Z. Fu, *Adv. Funct. Mater.*, 2020, **30**, 1909610.
7. C. Lin, P. Zhang, S. Wang, Q. Zhou, B. Na, H. Li, J. Tian, Y. Zhang, C. Deng, L. Meng, J. Wu, C. Liu, J. Hu and L. Zhang, *J. Alloys Compd.*, 2020, **823**, 153784.
8. L. Sha, J. Yin, K. Ye, G. Wang, K. Zhu, K. Cheng, J. Yan, G. Wang and D. Cao, *J. Mater. Chem. A*, 2019, **7**, 9078-9085.
9. Y. Ding, Q. Xue, Q. L. Hong, F. M. Li, Y. C. Jiang, S. N. Li and Y. Chen, *ACS Appl. Mater. Interfaces*, 2021, **13**, 4026-4033.
10. S. Sheng, K. Ye, L. Sha, K. Zhu, Y. Gao, J. Yan, G. Wang and D. Cao, *Inorg. Chem. Front.*, 2020, **7**, 4498-4506.
11. N. Jiang, B. You, R. Boonstra, I. M. Terrero Rodriguez and Y. Sun, *ACS Energy Letters*, 2016, **1**, 386-390.
12. C. Wang, H. Lu, Z. Mao, C. Yan, G. Shen and X. Wang, *Adv. Funct. Mater.*, 2020, **30**.
13. M. Li, X. Deng, K. Xiang, Y. Liang, B. Zhao, J. Hao, J. L. Luo and X. Z. Fu, *ChemSusChem*, 2020, **13**, 914-921.
14. M. Li, X. Deng, Y. Liang, K. Xiang, D. Wu, B. Zhao, H. Yang, J.-L. Luo and X.-Z. Fu, *J. Energ. Chem.*, 2020, **50**, 314-323.
15. Y. Xu, T. Ren, K. Ren, S. Yu, M. Liu, Z. Wang, X. Li, L. Wang and H. Wang, *Chem. Eng. J.*, 2021, **408**, 127308.
16. H. Zhou, Y. Ren, Z. Li, M. Xu, Y. Wang, R. Ge, X. Kong, L. Zheng and H. Duan, *Nat. Commun.*, 2021, **12**, 4679.
17. G. Liu, X. Zhang, C. Zhao, Q. Xiong, W. Gong, G. Wang, Y. Zhang, H. Zhang and H. Zhao, *New J. Chem.*, 2018, **42**, 6381-6388.